Identification of DNA 3′-Phosphatase Active Site Residues and Their Differential Role in DNA Binding, Mg^{2+} Coordination, and Catalysis†

Rajashree A. Deshpande and Thomas E. Wilson*

Department of Pathology, University of Michigan Medical School, 1301 Catherine Road, M4214 Medical Sciences Building I, Box 0602, Ann Arbor, Michigan 48109-0602

Received March 23, 2004; Revised Manuscript Received April 23, 2004

ABSTRACT: DNA 3′-phosphatase (Tpp1) from *Saccharomyces cerevisiae*, a homologue of human polynucleotide kinase/3′-phosphatase, has been shown to participate in DNA damage repair by removing 3′-phosphate blocking lesions. Tpp1 shows similarity to the L-2-haloacid dehalogenase superfamily of enzymes. By comparison to phosphoserine phosphatase, a well-studied member of this family, we designed conservative and nonconservative substitutions of likely active site residues of Tpp1 and tested them in a variety of assays. From the loss or impairment of activity, we identified D35, D37, T39, S88, K170, D206, and D218 as being involved in Tpp1 catalysis. D35 and K170 were the most critical since maximum inactivation was seen with even conservative mutations. Tpp1 bound DNA through its active site in a Mg^{2+}-dependent manner and exhibited a preference for dsDNA. Although Tpp1 bound more strongly to DNA with a free 3′ terminus, it also bound well to covalently closed DNA, suggesting a possible lesion scanning mechanism. DNA binding studies further indicated that Tpp1 coordinates Mg^{2+} through D35 and D206 and contacts the DNA 3′ end through D37. The removal of 3′-phosphate involved a phospho-Tpp1 intermediate, and our results support D35 as being the point of covalent attachment. On the basis of these similarities in mutant phenotypes of Tpp1 and phosphoserine phosphatase, we propose a reaction mechanism for Tpp1 which explains its strict phosphate specificity.

DNA strand breaks bearing abnormal termini, known as blocking lesions, arise through a continuous assault on the genome of living cells by various DNA damaging agents (*1*). Since these blocking lesions prevent the polymerization and ligation events that are necessary to reestablish the continuity of a DNA strand, removal of the abnormal termini is a prerequisite for DNA damage repair. All types of 3′ blocking lesions, e.g., 3′-phosphates, 3′-phosphoglycolates, and 3′-aldehydes, are removed by abasic endonucleases by virtue of their 3′-phosphodiesterase activity (*2*−*4*). In addition, many eukaryotes possess polynucleotide kinase (PNKP),[1] a bifunctional enzyme with 5′-kinase and 3′-phosphatase activities provided by two nonoverlapping catalytic domains (*5*−*7*). In budding yeasts, only the 3′-phosphatase activity is preserved in the form of DNA 3′-phosphatase (Tpp1), a protein with a high degree of sequence homology to only the phosphatase domain of PNKP (*8*) (Figure 1). Unlike the abasic endonucleases, Tpp1 exhibits strict specificity for 3′-phosphate lesions (*3*, *4*, *8*). In vivo, Tpp1 and the abasic endonucleases act redundantly in the removal of 3′-phosphate lesions left by oxidative damage, the enzyme Tdp1, and apparently other unknown sources (*3*, *4*).

Both Tpp1 and PNKP are members of the L-2-haloacid dehalogenase (HAD) superfamily of enzymes (*9*−*12*). Among the highly conserved regions of Tpp1 and PNKP are three HAD signature motifs known to form the active site in other members of this superfamily (*7*, *8*, *13*−*18*) (Figure 1). The absolutely conserved first aspartate of motif I (DxDxT/V) forms a covalent phosphoaspartate intermediate in several HAD phosphatases/phosphotransferases including phosphoserine phosphatase (PSP) (*19*), phosphomannomutase (*11*), cytosolic 5′-nucleotidase (*20*), and β-phosphoglucomutase (*21*). HAD motif II is centered around a conserved serine or threonine. HAD motif III (Kx_nG/DDx_nD) has strictly conserved lysine and aspartate residues separated by patches of less conserved residues. These three Tpp1 motifs show a strict alignment to PSP from *Methanococcus jannaschii* (Mj PSP), a well-studied member of the HAD superfamily whose crystal structure is available (*13*, *14*). The principal difference is a larger insertion between the conserved aspartates in Tpp1 motif III. Recently, crystal structures of human mitochondrial 5′-deoxyribonucleotidase (dNT2) (*15*) and RNA polynucleotide kinase from T4 bacteriophage (T4 PNK) (*16*) were also solved and the proteins shown to be structural members of the HAD superfamily. Although both of these enzymes possess a nucleotide phosphatase activity, neither is DNA-specific like Tpp1. Indeed, T4 PNK shows a low sequence homology with Tpp1, and dNT2 does not share any similarity aside from the HAD motifs. Similarly, dNT2 and T4 PNK show little sequence similarity to PSP, even though their crystal structures show similar folding and nearly superimposable active site residues. This divergence is most evident

† This work was supported by the Pew Scholars Program in the Biomedical Sciences of the Pew Charitable Trusts and U.S. Public Health Service Grant CA-90911 (to T.E.W.).

* To whom correspondence should be addressed. Phone: (734) 936-1887. Fax: (734) 763-6476. E-mail: wilsonte@umich.edu.

[1] Abbreviations: PNKP, polynucleotide kinase/3′-phosphatase; HAD, L-2-haloacid dehalogenase; PSP, phosphoserine phosphatase; PNK, polynucleotide kinase; UDG, uracil DNA glycosylase; EMSA, electrophoretic mobility shift assay; GST, glutathione *S*-transferase.

10.1021/bi049434n CCC: $27.50
Published on Web 05/29/2004

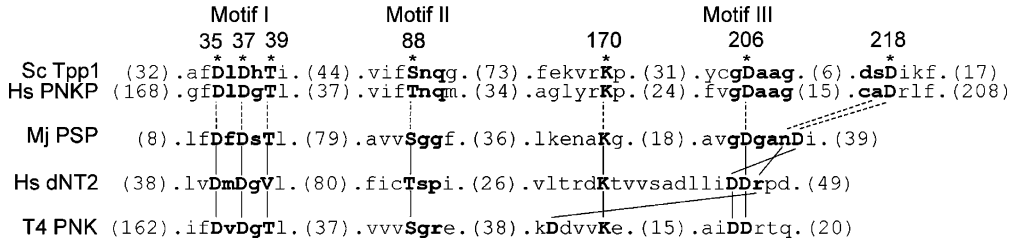

FIGURE 1: Relationship of mutated Tpp1 residues to motifs characteristic of the L-2-haloacid dehalogenase (HAD) superfamily. Phosphoserine phosphatase from *M. jannaschii* (Mj PSP), human mitochondrial 5′-deoxyribonucleotidase (Hs dNT2), and T4 polynucleotide kinase (T4 PNK) are phosphatases of the HAD superfamily with known structures (*13*−*16*). The regions from their sequences containing the catalytic residues (in upper case) are shown, with numbers in parentheses indicating the number of amino acids separating the adjoining regions. The catalytic residues that are inferred from the crystal structures of PSP, dNT2, and T4 PNK to have the same position and functional role are connected by solid lines. These catalytic residues constitute three motifs (in bold) which are characteristic of the HAD superfamily (*9*−*12*). Tpp1 from *S. cerevisiae* (Sc Tpp1) exhibits high sequence similarity to the 3′-phosphatase domain of human polynucleotide kinase (Hs PNKP) (*8*), and regions from their sequences which were identified as HAD superfamily motifs are aligned. Broken lines connect the Tpp1 and Hs PNKP residues that correspond to the catalytic residues of Mj PSP. Tpp1 residues numbered and marked with an asterisk were mutated in this study.

in motif III where amino acids with the same functional role do not show primary structure alignment between dNT2, T4 PNK, and Mj PSP (Figure 1). Thus, at least with respect to its primary structure, Tpp1 appears to be more related to PSP rather than dNT2 or T4 PNK.

The active site residues of Mj PSP, as a prototypic example, are arranged to form sites for binding of Mg^{2+} and phosphate (Figure 9). Mg^{2+} is critical for activity and is coordinated by PSP D11 and D167 side chains, the main chain carbonyl group of D13, the phosphate, and two water molecules. The phosphate is bound by side chains of D13, S99, K144, and Mg^{2+}. K144 and Mg^{2+} are the only positively charged groups in the active site and serve to neutralize the phosphate negative charge. D13 acts as a general acid that donates a proton to stabilize the negative charges developed on the apical oxygen atom upon scissile bond cleavage, mediated by nucleophilic attack of D11 on the phosphate. Deprotonated D13 subsequently acts as a general base, activating a water molecule responsible for hydrolysis of the phosphoaspartate intermediate (*13*, *14*).

Since Tpp1 has HAD motifs which closely resemble those of Mj PSP, we hypothesize that Tpp1 has a catalytic mechanism similar to that of the HAD superfamily, especially PSP. However, unlike any other known HAD superfamily protein, a 3′-phosphatase must engage DNA as part of its catalytic cycle. Binding to a highly charged macromolecule not only places unique demands on the protein and its active site but also allows for the application of facile experimental approaches not generally possible with small molecule substrates. Here we explore these hypotheses using site-directed mutagenesis. Using in vivo and in vitro activity assays in conjunction with in vitro DNA binding assays, we establish the contribution of seven different amino acids to catalysis, substrate binding, Mg^{2+} coordination, and formation of a covalent phospho-Tpp1 intermediate. These findings are discussed in the context of the known functional properties of this DNA repair enzyme.

EXPERIMENTAL PROCEDURES

Yeast Strains. Creation of *Saccharomyces cerevisiae* strain YW950 (*MAT*α *can*1Δ::Myc-Fpg *apn*1Δ::*HIS*3 *apn*2Δ::*kanMX4 tpp*1Δ::*MET*15 *ade*2Δ0 *his*3Δ200 *leu*2 *met*15Δ0 *trp*1Δ63 *ura*3Δ0) was described in Karumbati et al. (*4*). *S. cerevisiae* strain YW607/EJ758 (*MAT*a *his*3Δ200 *leu*2-3, 112 *pep4*::HIS3 *ura*3-52) was used for expressing GST fusion protein cassettes (*22*).

Tpp1 Expression Plasmids and Mutagenesis. pTW375 is a *LEU2*/*CEN*/*ARS* vector that expresses His_9-Myc_3-Tpp1 from the strong constitutive *ADH*1 promoter, and its creation was described in Karumbati et al. (*4*). D35A and D37A mutants were described in Karumbati et al. (*4*). pTW375 served as a template for creating additional Tpp1 point mutations using the QuikChange multi-site-directed mutagenesis kit (Stratagene). Positive clones were detected by diagnostic PCR and sequenced to confirm the expected mutation as well as to rule out the introduction of additional mutations. Plasmids expressing wild-type and mutant Tpp1 as GST fusion proteins were created by gap repair cloning into modified pYEX 4T-1 (*22*). *Eco*RI/*Sma*I digested, modified pYEX 4T-1 was cotransformed into YW607 with PCR fragments corresponding to the Tpp1 coding sequence possessing 5′ tails homologous to the recombination domain of pYEX 4T-1 (5′-TTCGATGATGAAGATACCCCAC-CAAACCCAAAAAAAGAGATCGAAAT and 5′-TTCAG-TATCTACGATTCATAGATCTCTGCAGGTCGACGG-ATCCCCCT for the amino- and carboxyl-terminal sides, respectively.)

Measurement of Drug Sensitivity. pTW375 and its mutant derivatives were transformed into YW950, and their drug sensitivity was measured as described previously (*4*). Exponentially growing cells were exposed to varying concentrations of MMS in 50 mM potassium phosphate buffer, pH 7.5, at 30 °C for 30 min with shaking. Survival was determined by plating serial dilutions to leucine-selective plates and counting colonies following incubation at 30 °C for 3−4 days.

Western Blotting. Expression of His_9-Myc_3-Tpp1 derivatives was determined by boiling 0.5 OD_{600} cells in SDS−PAGE sample loading buffer followed by electrophoresis on 10% SDS−PAGE and transfer to nitrocellulose membrane. Blots were developed using mouse anti-cMyc (Santa Cruz) and alkaline phosphatase-conjugated rabbit anti-mouse secondary antibodies (Sigma).

Oligonucleotide Substrates. Oligonucleotides used in these studies are shown in Figure 4. The duplex oligonucleotide bearing a 3′-phosphate at a 1-nt gap (O10) used for Tpp1 activity assays and its labeling and annealing were as described (*8*). Oligonucleotide O1 is a 14-nt ssDNA which

does not have any predicted secondary structure. O2 is a perfect hairpin, derived from O1, with a 10-nt stem and a 5-nt loop. O3 was derived by addition of an 11-nt tail onto the 5′ terminus of O2. The sequence of this tail was designed so that it neither self-anneals nor anneals to the sequence in the stem. O4 has the same sequence as O3 but carries a phosphate group at the 3′ end. O5, which has a 5′-uracil residue, is structurally similar to O3 but has a totally different sequence; in addition, its 5′ tail is complementary to the 5′ tail of O3. O6 was created by ligating 5′ radiolabeled O3 and nonphosphorylated O5, leaving a nick in the perfectly base-paired stem. O7 was created similarly except that O5 was 5′-phosphorylated, so that ligation results in a closed circular molecule. O8 and O9 were obtained by ligating 5′ radiolabeled O3 to oligonucleotides which have essentially the same sequence as O5 but were 1 and 3 nt shorter at the 5′ terminus, so that O8 and O9 have a 1-nt and 3-nt gap, respectively. All ligation products were purified by passive elution from slices of a 7 M urea and 12% polyacrylamide gel and reannealed by heating to 95 °C and slow cooling prior to use. The presence of a single reannealed species of the predicted size was confirmed by 8% nondenaturing PAGE.

DNA with radioactive phosphate at the 3′ terminus was created as follows. O5 was radiolabeled at its 5′ end with [γ-^{32}P]ATP and then ligated to O3. An abasic site was created in the ligated product by treatment with uracil DNA glycosylase (UDG). This apyrimidinic DNA was then boiled at 95 °C for 30 min after the pH was increased to 10.5 by addition of 1 N NaOH. This treatment resulted in β and δ elimination reactions at the abasic site (*23*−*26*), leading to a break in the DNA backbone such that the radioactive phosphate was now present at the 3′ end of O3. The presence of radioactive phosphate at the 3′ terminus was confirmed by the loss of signal in denaturing gels upon treatment with wild-type Tpp1. The final product with 3′ radioactive phosphate was purified on denaturing gels as described above.

Enzyme Activity Assays. GST-Tpp1 derivatives were overexpressed and purified from yeast cells as described (*8*), and protein was estimated from SDS−PAGE gels stained with Coomassie blue using BSA as a standard. 3′-Phosphatase activity assay using a duplex oligonucleotide bearing a 3′-phosphate at a nick was carried out essentially as described (*8*). The reaction mixture contained 50 fmol of DNA substrate and appropriate amounts of enzyme in a volume of 10 μL such that the final assay buffer was 50 mM Tris-HCl (pH 7.5), 100 mM NaCl, 10 mM $MgCl_2$, 1 mM DTT, and 50 μg/mL BSA. After incubation at 30 °C for 30 min, the reaction was stopped by addition of formamide/EDTA loading buffer, and samples were electrophoresed on 7 M urea and 12% polyacrylamide gels followed by autoradiography or phosphorimaging and analysis using Imagequant software (Amersham).

Electrophoretic Mobility Shift Assay (EMSA). For oligonucleotides, 100 fmol of DNA was incubated with 500 fmol of enzyme in 10 μL of assay buffer (described above) at 30 °C for 30 min. Loading buffer (50% glycerol in assay buffer) was added, and the samples were electrophoresed on 4% acrylamide gels in 0.5× TB (TBE lacking EDTA) at 60 V and room temperature. To examine the role of Mg^{2+} in DNA binding, $MgCl_2$ was omitted and 20 mM EDTA was added to the assay buffer, and these samples were electrophoresed with 0.5× TBE. Gels were dried, phosphorimaged, and analyzed using Imagequant software.

For plasmids, 150 ng of pES16 (*27*) was incubated with increasing amounts (3−24 pmol) of wild-type Tpp1 in 30 μL of assay buffer at room temperature for 5 min. Ten microliters of the reaction was mixed with 2 μL of loading buffer and electrophoresed on 0.8% agarose in 1× TA (TAE lacking EDTA) at room temperature. The remaining 20 μL was extracted with phenol−chloroform, and 10 μL of the aqueous phase was mixed with loading buffer and electrophoresed similarly. Gels were stained after electrophoresis with 0.5 μg/mL ethidium bromide. To examine the role of Mg^{2+} in DNA binding, $MgCl_2$ was omitted and 20 mM EDTA was added to the assay buffer, and these samples were electrophoresed with 1× TAE buffer.

Detection of the Phospho-Tpp1 Intermediate. Enzyme (4.5 pmol) was incubated with 400 fmol of DNA substrate bearing a 3′ radioactive phosphate in 10 μL of assay buffer at 4 °C for 30−40 s, and the reaction was stopped with rapid mixing into SDS−PAGE sample loading buffer. Samples were loaded on 0.1% SDS and 10% polyacrylamide gels without heat denaturing and electrophoresed at 94 V in an ice bath with SDS omitted from the lower tank buffer. Prestained protein molecular weight markers were loaded in two lanes. Prior to fixing, the gel was cut to separate the highly radioactive bottom part, corresponding to the substrate, from the upper part where the enzyme would migrate. The upper part was further cut into two parts. One part, containing one marker lane, was used for phosphorimaging after fixing in methanol−acetic acid−water (40:10:50) and vacuum drying at 45 °C for 2−3 h. The other part, with the other marker lane, was used for Coomassie staining. After imaging, the images were sized and aligned to each other using the marker lanes.

RESULTS

Mutation of Tpp1 HAD Motifs Abolishes 3′-Phosphatase Activity in Vivo and in Vitro. The striking similarity of the conserved HAD motifs and invariable aspartates between Tpp1 and Mj PSP pointed to a similar functional role for these residues in the Tpp1 reaction mechanism. To investigate this possibility, we carried out site-directed mutagenesis and replaced the conserved Tpp1 residues D35, D37, T39, S88, K170, D206, and D218 with both conservative and nonconservative alanine substitutions. The effect of these mutations on Tpp1 function was first assessed using an in vivo assay described previously (*4*) and depicted in Figure 2A. The assay relies on conversion of abasic sites created after MMS treatment into 3′-phosphate blocking lesions by bacterial Fpg expressed in yeast. Because the yeast strain also lacks the abasic endonucleases Apn1 and Apn2, survival following MMS treatment is strictly dependent on functional Tpp1. Transformants carrying empty vector plasmids showed 3800-fold less survival as compared to plasmids expressing wild-type Tpp1 (*4*) (Figure 2C). The survival of transformants carrying plasmids expressing alanine replacements of the four invariable aspartates, D35, D37, D206, and D218, and K170 was similar to the vector only transformants (Figure 2C). Moreover, a similar poor survival was also seen with the conservative substitutions D35N, D35E, D218E, and

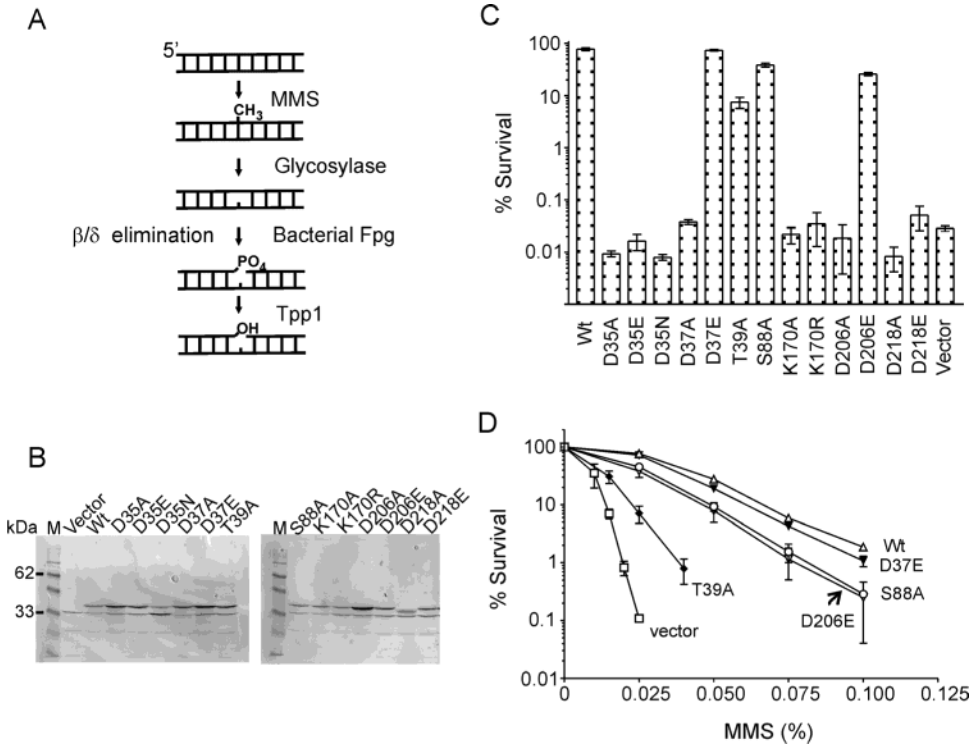

FIGURE 2: Tpp1 HAD motif mutants are severely impaired in 3′-phosphate removal in vivo. (A) Schematic of the in vivo assay for function of Tpp1. Plasmids expressing Tpp1 or its mutant derivatives were transformed in YW950 (*can1*Δ::Myc-Fpg *apn1 apn2 tpp1*). Treatment of these transformants with MMS results in methylation of bases. Removal of these modified bases by glycosylases leads to abasic sites, which, in the absence of Apn1 and Apn2, are cleaved by bacterial Fpg into strand breaks with 3′-phosphates, the substrate for Tpp1. Only when active Tpp1 is present are 3′-hydroxyl ends generated, allowing lesion repair and cell survival (*4*). (B) Detection of Tpp1 expression levels in YW950 transformants by Western blotting using anti-cMyc antibodies. A band corresponding to 43 kDa His_9-Myc_3-Tpp1 was seen in all mutants, except the vector only lane, whereas the 33 kDa Myc-Fpg band is present in all lanes and serves as a loading control. (C) Sensitivity of YW950 transformants to 0.025% MMS. (D) Sensitivity of wild-type Tpp1 and select mutants to varying concentrations of MMS.

K170R. On the other hand, the conservative substitutions D37E, T39A, S88A, and D206E improved survival to variable extents. Survival with the D37E mutant was comparable to that of wild-type Tpp1, even at MMS concentrations higher than 0.025% (Figure 2D). As seen in Western blots, all mutants, except D218A, expressed a 43 kDa cMyc-tagged full-length protein at levels either comparable to or higher than wild-type Tpp1 (Figure 2B). Because D218A showed no other mutation or truncation in the gene upon repeated sequencing of recovered plasmid, we attribute its faster migration to an unknown conformational effect. The poor survival of all mutants could be attributed to loss of Tpp1 3′-phosphatase activity due to the substitutions since even the higher expression levels observed with some mutants were unable to complement Tpp1 deficiency.

The results obtained with the in vivo assay were corroborated by the in vitro estimation of catalytic activity. Wild-type Tpp1 and all mutants were expressed as GST fusion proteins and purified as full-length (56 kDa) proteins (Figure 3A). Only D37E, S88A, and D206E were capable of removing a 3′-phosphate when 100 fmol of enzyme was used, which is 10-fold higher than the amount required for complete removal of 3′-phosphate by wild-type Tpp1 under similar conditions (Figure 3B). Indeed, quantitation of the activity with increasing amounts of D37E, S88A, and D206E mutants showed severely impaired 3′-phosphatase activity (Figure 3D). From the remaining mutants, only D35E, D37A, D206A, D218A, and T39A displayed some activity when a very high amount of protein (5000 fmol) was used, whereas D35A, D35N, K170A, K170R, and D218E did not show any activity (Figure 3C). Importantly, the very low activity exhibited by T39A, K170A ,and K170R overruled any contribution to enzymatic activity by contaminating bands seen in these mutants (Figure 3A).

In total, the results from in vivo and in vitro assays showed a direct correlation in the relative pattern of activity of mutants. The in vivo assay appears to be less sensitive to Tpp1 mutant defects, however. This is likely a result of overexpression from the strong ADH promoter, coupled with a longer incubation period allowing more time for repair. Taken together, the complete loss or partial impairment of activity of Tpp1 mutants indicates the importance of the mutated residues in Tpp1 catalysis. In particular, D35 and K170 are essentially indispensable. These results strongly support the hypothesis that the targeted residues either form the active site or are very close to the active site.

Tpp1 Binds to DNA through Its Active Site. In addition to catalytic defects, the loss of enzymatic activity seen with Tpp1 mutants could reflect an inability to engage substrate or cofactor in the active site. We carried out DNA binding studies using EMSA to explore this. We first used oligonucleotide substrates which self-anneal and possess only one 5′ and 3′ end. These carried either a 3′-hydroxyl (Figure 4, O3) or 3′-phosphate (O4). In the presence of Mg^{2+}, wild-type Tpp1 and D35A each showed formation of a stable DNA−enzyme complex, as indicated by a strong shifted band (Figure 5). Wild-type Tpp1 showed equal binding to

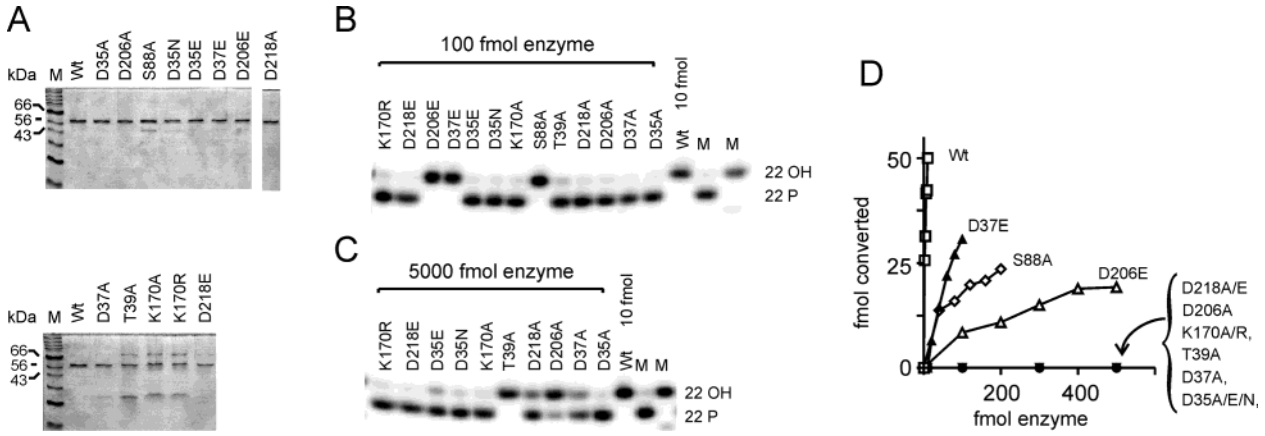

FIGURE 3: Tpp1 HAD motif mutants are severely impaired in 3′-phosphate removal in vitro. (A) Wild-type Tpp1 and mutant derivatives (56 kDa) were purified as GST fusion proteins, and the purity of the preparation was determined by 10% SDS−PAGE. For the top panel and wild type in the bottom panel, 0.2 μg of GST-Tpp1 was loaded whereas 0.1 μg of GST-Tpp1 was used for mutants in the bottom panel. Note that K170A and K170R migrated a bit slowly due to a larger loading volume and therefore higher glycerol content whereas D218A migrates slightly faster (similar to Western blots). (B) 50 fmol of DNA substrate was incubated with 10 fmol wild-type Tpp1 or 100 fmol of mutants at 30 °C for 30 min, and the products were separated on a 7 M urea and 12% acrylamide gel and autoradiographed. The 22-mer oligonucleotide synthesized with and without a 3′-phosphate served as markers (lanes M). (C) Similar to (B) except with 100 fmol of substrate and 5000 fmol of enzyme. (D) 50 fmol of DNA substrate was incubated with the indicated amounts of enzyme, and the reaction products were separated by denaturing PAGE followed by phosphorimaging and quantification using Imagequant software.

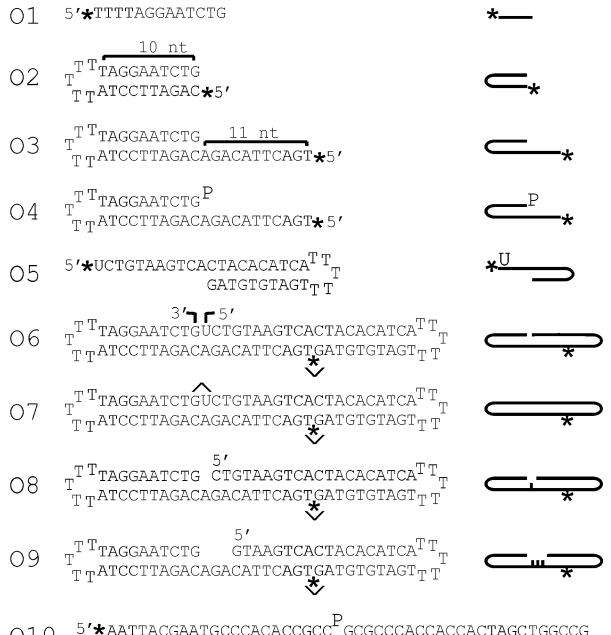

FIGURE 4: Oligonucleotides used for DNA binding studies. O1−O5 were synthesized, and O6−O9 were prepared by ligation (details in Experimental Procedures). Asterisks indicate the position of the ^{32}P label, ∧ represents the point of ligation, and P indicates a 3′-phosphate group.

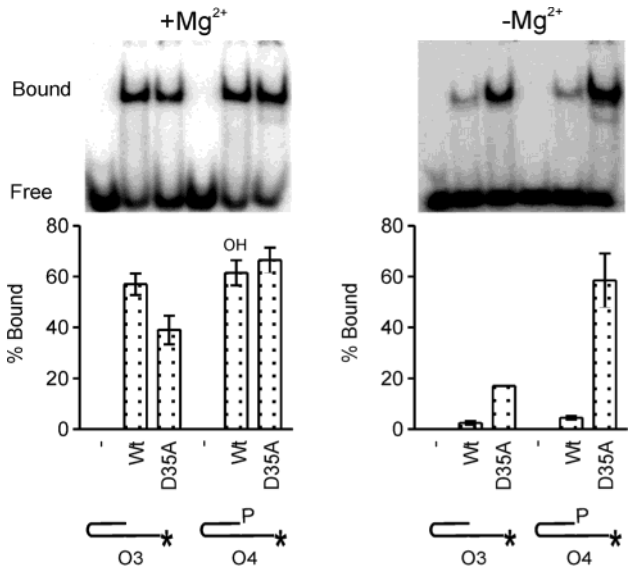

FIGURE 5: Tpp1 exhibits stable Mg^{2+}-dependent binding to DNA through its active site. EMSA was performed using 500 fmol of either wild-type Tpp1 or D35A and 100 fmol of the indicated DNA in the presence (left panel) or absence (right panel) of Mg^{2+}, as described in Experimental Procedures. The amount of substrate shifted was quantified and is presented graphically below the autoradiograms. Note that, in the presence of Mg^{2+} and active Tpp1, all of the 3′-phosphate substrate is hydrolyzed to 3′-hydroxyl, and the band essentially represents binding to 3′-hydroxyl. This is indicated by the letters OH above the relevant bar.

both 3′-hydroxyl and 3′-phosphate. This was not surprising, since under the assay conditions active Tpp1 catalyzes removal of the 3′-phosphate to leave a 3′-hydroxyl. With the 3′-hydroxyl substrate, D35A showed ∼1.5-fold less binding than wild-type Tpp1. D35A binding to the 3′-phosphate substrate was ∼2-fold more as compared to 3′-hydroxyl, suggesting that specific contacts are made to the 3′-phosphate.

To study the role of Mg^{2+} in substrate binding, $MgCl_2$ was omitted and 20 mM EDTA was included in the assay buffer. Under these conditions, catalytic activity of wild-type Tpp1 was abolished as expected (*8*). In parallel with this, binding to both 3′-hydroxyl and 3′-phosphate substrates was also severely diminished. In marked contrast, D35A still showed strong binding to both 3′-hydroxyl and 3′-phosphate in the absence of Mg^{2+}, albeit at a reduced level with the 3′-hydroxyl. These results demonstrate a crucial role for Mg^{2+} in DNA binding by the wild-type enzyme, which in turn strongly suggests that this binding occurs through the Tpp1 active site. This conclusion is further supported by the suppression of Mg^{2+} dependence by the D35A active site mutation.

Tpp1 Binds Preferentially, but Not Exclusively, to dsDNA with Free Ends. Binding studies were extended to further study the dependence of Tpp1 binding on DNA structure.

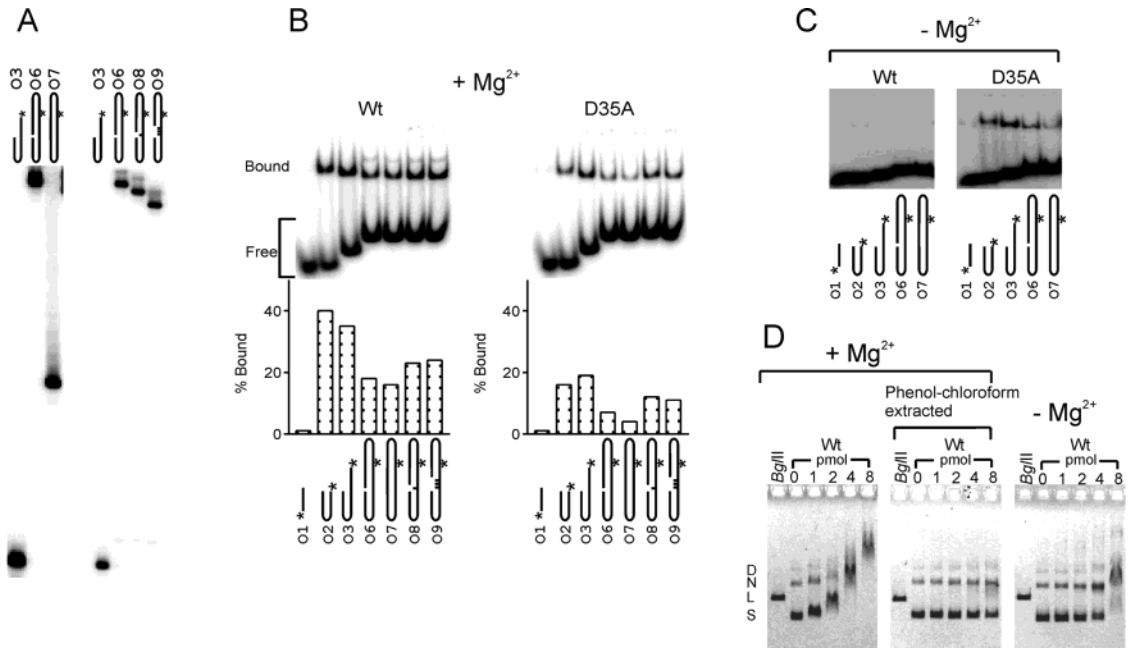

FIGURE 6: Tpp1 binds preferentially to dsDNA with free ends. (A) A 7 M urea and 12% acrylamide denaturing gel shows the different migration of the indicated oligonucleotides obtained following ligation of O3 and O5 (shown in Figure 4). Samples in the left panel were run after PAGE purification. Samples in the right panel were run prior to purification, and so a small amount of starting material is seen. (B, C) EMSA was carried out using 500 fmol of either wild-type Tpp1 or D35A and 100 fmol of purified oligonucleotides in the presence (B) or absence (C) of Mg^{2+}. Electrophoresis was carried out on a 4% native polyacrylamide gel followed by phosphorimaging and analysis using Imagequant software. (D) 150 ng of plasmid pES16 was incubated with increasing amounts of wild-type Tpp1 in the presence of Mg^{2+} at room temperature for 5 min. Samples containing 50 ng of pES16 were electrophoresed on 0.8% agarose in 1× TA buffer before phenol−chloroform extraction (left panel) or after extraction (middle panel). The right panel shows the migration of DNA when the reaction was carried out in the absence of Mg^{2+} at room temperature for 5 min. pES16 linearized with *Bgl*II was used as a marker, and the different plasmid species are indicated as S (supercoiled), L (linear), N (nicked circular), and D (dimer).

The various substrates used (Figure 4) were prepared by ligating different synthetic oligonucleotides, and the presence of the expected ligation product was confirmed by denaturing PAGE (Figure 6A). The presence of the covalently closed structure (O7) was confirmed by a band migrating faster than the nicked molecule (O6) but slower than the starting oligonucleotide, O3. In the presence of Mg^{2+}, both wild-type Tpp1 and D35A displayed a similar pattern of binding, although D35A again bound ~2-fold less than wild type (Figure 6B). The enzymes showed very poor binding to ssDNA as opposed to the strong binding to oligonucleotides with dsDNA, explaining our previous observation that ssDNA is a poor substrate for Tpp1 (*8*). Among the dsDNA substrates, highest binding was observed with oligonucleotides with a free end (O2 and O3). A terminus was not a prerequisite for binding, however, as demonstrated by binding to the covalently closed structure (O7). Surprisingly, a nick in the circular substrate (O6) was not sufficient to restore the highest level of binding, suggesting an inhibition by the 5′-terminated strand at the nick. The introduction of a 1-nt or 3-nt gap in the circular DNA (O8 and O9, respectively) partially relieved this inhibition, although binding was still submaximal. In lanes with O6−O9, the primary shifted band migrated faster than with O2 and O3, which is a result of the increased charge/mass ratio in Tpp1 complexes with longer oligonucleotides. Moreover, an additional band appeared in these lanes, which is most likely due to binding of multiple Tpp1 molecules. In the absence of Mg^{2+}, wild-type Tpp1 was essentially unable to bind any of the substrates whereas D35A again retained substantial binding (Figure 6C).

The surprising ability of Tpp1 to bind strongly to covalently closed DNA was confirmed using agarose gel EMSA and a supercoiled plasmid. In the presence of Mg^{2+}, a shift in the electrophoretic mobility of the plasmid was observed with wild-type Tpp1, which was lost after removal of protein from the reaction mixture by phenol−chloroform extraction (Figure 6D). Importantly, the DNA retained the same degree of supercoiling after exposure to Tpp1, proving the binding of Tpp1 to terminus-free DNA. As with oligonucleotides, the progressive plasmid shift at increasing Tpp1 concentrations demonstrates the binding of many Tpp1 molecules per plasmid. In the absence of Mg^{2+}, binding was again strongly inhibited.

Active Site Residues Contacting Mg^{2+} and the 3′ Terminus of DNA. We next asked whether other active site mutants could bind DNA and whether the binding was Mg^{2+}-dependent (Figure 7). When compared to D35A, D35N behaved similarly and exhibited a preference for 3′-phosphate and relative Mg^{2+} independence, although binding was not as strong as D35A. The binding was reduced even more when glutamate replaced D35 so that D35E was now essentially unable to bind. The behavior of D206 mutants was similar to D35 mutants. D206E displayed drastically reduced binding under all conditions, while D206A showed Mg^{2+}-independent binding to both 3′-hydroxyl and 3′-phosphate. D206A did not exhibit an apparent preference for a 3′-phosphate, however, in contrast to D35A. These patterns are consistent with both a role of D35 and D206 in Mg^{2+} binding and a role for Mg^{2+} in charge stabilization in the active site (see Discussion). We note that although D35A, D35N, and D206A exhibited Mg^{2+} independence, binding

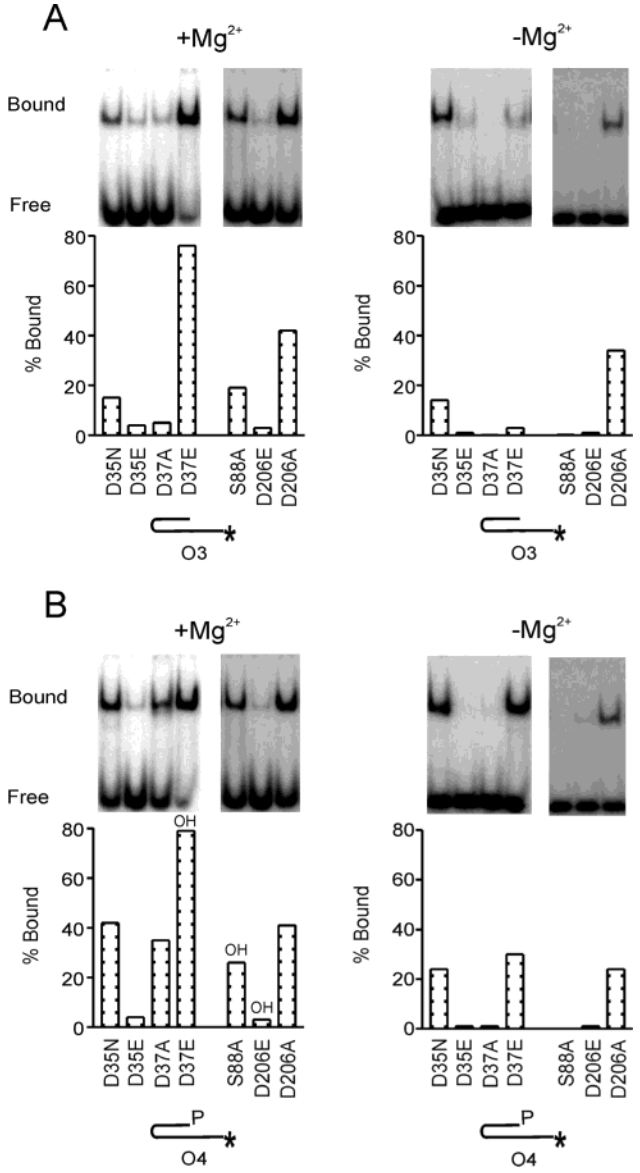

FIGURE 7: Active site residues contacting Mg^{2+} and the 3′ terminus of DNA. EMSA was performed in the presence and absence of Mg^{2+} as described for Figure 5. All of the 3′-phosphate substrate is hydrolyzed to 3′-hydroxyl in the presence of Mg^{2+} and active enzyme (indicated by OH above the bars). Note the strikingly different patterns seen for D35 and D206 mutants as compared to D37 mutants.

in the presence of Mg^{2+} was generally better than in its absence, suggesting that these single mutants retain some Mg^{2+} binding capacity.

A completely different picture was seen with D37 mutants. In contrast to D35, D37A could not effectively bind 3′-hydroxyl DNA, even in the presence of Mg^{2+}, whereas D37E showed a very strong binding with a strong requirement for Mg^{2+}. With the 3′-phosphate substrate, D37A now showed Mg^{2+}-dependent binding. Most strikingly, D37E bound well to a 3′-phosphate even in the absence of Mg^{2+}. It is again not meaningful to study D37E binding to 3′-phosphate in the presence of Mg^{2+}, as this active mutant will cleave the phosphate. Collectively, this pattern is consistent with a role of D37 in contacting the 3′ terminus (see Discussion).

S88A showed a totally Mg^{2+}-dependent binding to 3′-hydroxyl DNA, similar to its relatively high preservation of

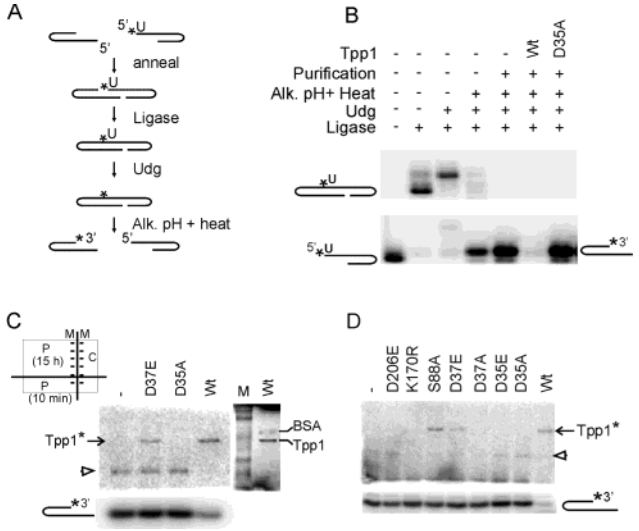

FIGURE 8: Detection of a covalent phospho-Tpp1 intermediate. (A) Schematic of the preparation of an oligonucleotide with 3′ radioactive phosphate by transfer from a 5′-phosphate (for details see Experimental Procedures). (B) Samples at every stage of radiolabel transfer were electrophoresed on 7 M urea and 12% polyacrylamide gel (only the top and bottom gel portions are shown for space), and where indicated, samples were treated with wild-type Tpp1 or D35A. (C) The phopsho-Tpp1 intermediate (Tpp1*) was detected by incubating 400 fmol of 3′ radioactive phosphate substrate with 4.5 pmol of enzyme at 4 °C for 30−40 s, followed by electrophoresis on 0.1% SDS and 10% acrylamide gel. The inset shows how the gel was cut. P and C indicate subsequent phosphorimaging and Coomassie brilliant blue staining, respectively, and M indicates prestained molecular weight markers that were used to align the final images. The left top (protein) and bottom (substrate) parts were exposed to a phosphorimager screen for 15 h and 10 min, respectively. (D) Detection of the phospho-Tpp1 intermediate was carried out with the indicated mutants as in (C). Note in (C) and (D) that the degree of substrate cleavage during the reaction can be judged from the bottom portion of the gel. An open arrowhead denotes a band whose presence correlates directly with the extent of residual substrate. Because it appears even in the absence of protein, this band is inferred to be a minor alternative conformation of the DNA substrate.

catalytic activity. Other mutants, T39A, K170A, K170R, D218A, and D218E, did not show binding to either 3′-hydroxyl and 3′-phosphate substrates in the presence of Mg^{2+} (data not shown).

Tpp1 Catalysis Entails Transfer of the 3′-Phosphate to a Covalent Phospho-Tpp1 Intermediate. With the active site residues identified as the highly conserved residues from the HAD superfamily motifs, it was almost certain that the catalytic mechanism of Tpp1 resembles that of Mj PSP. To prove this unequivocally, we sought to detect the presence of a covalent intermediate of Tpp1 with the leaving phosphate group. We created a substrate carrying a radioactive phosphate at its 3′ end by transferring a 5′-^{32}P radiolabel from one oligonucleotide to the 3′ end of another (see Figure 8A and Experimental Procedures). The migration of reaction intermediates and products on denaturing PAGE revealed the expected changes in oligonucleotide length following ligation, UDG treatment, and heat treatment in alkaline conditions. Moreover, disappearance of the radioactive signal on treatment with Tpp1, but not D35A, confirmed the presence of a 3′ radioactive phosphate (Figure 8B). The detection of the phospho-Tpp1 intermediate required high concentrations of both the enzyme and substrate, short assay

Table 1: Summary of Tpp1 Mutant Phenotypes and Their Comparison with Human PSP

	Tpp1							
	activity[a]		3′-hydroxyl binding		3′-phosphate binding		phospho-Tpp1	hPSP[b]
	in vivo	in vitro	+Mg	−Mg	+Mg	−Mg		
wild type	++	++	+	−	NA[c]	−	+	
D35A	−	−	+	+	+	+	−	
D35E	−	−	−	−	−	−	−	D20E (−)
D35N	−	−	+	+	+	+	ND[d]	D20N (−)
D37A	−	±	−	−	+	−	−	D22N (−)
D37E	++	+	+	−	NA	+	+	D22E (+)
T39A	+	±	−	ND	−	ND	−	
S88A	+	+	+	−	NA	−	+	S109A (+)
K170A	−	−	−	ND	−	ND	ND	K158A (±)
K170R	−	−	−	ND	−	ND	−	K158R (±)
D206A	−	±	+	+	+	+	−	D179N (±)
D206E	+	+	−	−	NA	−	−	D179E (+)
D218A	−	±	−	ND	−	ND	ND	D183N (±)
D218E	−	−	ND	ND	ND	ND	ND	D183E (+)

[a] For activity, ++ indicates wild-type levels, + indicates reduced but easily detectable levels, and ± indicates activity only at very high enzyme concentration. [b] Mutations of the corresponding residues from hPSP; loss or retention of activity is indicated in parentheses. See ref *19*. [c] NA = not applicable; these enzymes cleaved the 3′-phosphate in the presence of Mg^{2+} during the binding reaction. [d] ND = not done.

duration, and low temperature, which is consistent with the known lability of phosphoaspartate bonds (*28*−*30*). Following SDS−PAGE, wild-type Tpp1 as well as the active mutant D37E showed a radioactive signal band at the same position as GST-Tpp1 (Figure 8C). The absence of such a band in the lane with catalytically inactive D35A proves that this band was arising through an enzymatic transfer of radiolabel to Tpp1. Moreover, the absence of a band at the position corresponding to BSA (which is seen in the Coomassie-stained gels) and the stability of the signal under denaturing conditions confirm a Tpp1-specific covalent complex with the radioactive phosphate.

In addition to wild-type Tpp1 and D37E, S88A was the only other catalytically active mutant which showed the phospho-Tpp1 intermediate (Figure 8D). The maximum yield of phosphoaspartate was seen with S88A whereas D37E exhibited a consistently lower yield than wild-type Tpp1 and S88A. It is most notable that D206E failed to show complex formation despite significant residual activity. The covalent intermediate was not detected with the severely impaired mutants D35A/E, D37A, T39A, K170R, D206A, and D218A even when the reaction time and temperature were varied (Figure 8D; data not shown). This suggests that hydrolysis of the Tpp1-bound phosphate is not the rate-limiting step for these mutants.

DISCUSSION

Tpp1 Belongs to the HAD Superfamily. By comparison with the HAD superfamily of enzymes, and PSP in particular, we have designed conservative and nonconservative substitutions of likely Tpp1 active site residues and assessed their effect both in vivo and in vitro. The activity pattern of these mutants was very similar to that observed previously for human PSP (hPSP), especially among mutants that retained some activity (*11*, *19*) (Table 1). Comparison to T4 PNK was less informative due to the lower correspondence of its catalytic residues (Figure 1) and the fact that its active site mutations are more uniformly disabling (*31*). In HAD family members the first aspartate in motif I is invariable and the most critical (*9*−*12*, *19*, *32*). Similarly, the first aspartate in Tpp1 motif I, D35, proved to be indispensable for activity. The second aspartate in motif I, D37, was not as critical since its substitution by glutamate retained substantial activity. This mimics hPSP, and indeed, in some species glutamate is naturally observed at this position in PSP (*11*, *13*, *19*). The D37 side chain was important, however, given the nearly total loss of activity with alanine substitution. Subtle differences were seen with other residues, for example, Tpp1 mutants D218A and K170R (Table 1). In total, however, the striking similarity between our Tpp1 functional analysis and those reported previously for PSP and T4 PNK (*11*, *19*, *31*) strongly supports the correspondence of their HAD motifs as illustrated in Figure 1. On the basis of this, we present a model of the active site and catalytic mechanism of Tpp1 (Figure 9) that is similar to those proposed for PSP, T4 PNK, and dNT2 (*11*, *14*−*16*, *19*, *31*) and explored in detail below.

Formation and Hydrolysis of the Phospho-Tpp1 Reaction Intermediate. Phosphatases from the HAD superfamily utilize a two-step reaction mechanism involving (i) formation of a covalent phosphoenzyme intermediate through nucleophilic attack by the first conserved aspartate from motif I and (ii) its subsequent degradation by an activated water molecule (*13*−*15*). We have demonstrated a covalent phospho-Tpp1 intermediate, providing further evidence of a common reaction mechanism with PSP. Beyond the inference from HAD homology, our results support that this complex is formed through D35. We were unable to detect the intermediate with any D35 mutant, and D35A showed an absolute loss of 3′-phosphatase activity despite retention of strong substrate binding. In contrast, direct visualization of the covalent intermediate and/or retention of at least minimal residual activity by all other active site alanine replacements eliminated those residues as being the point of covalent attachment. The failure to detect the phospho-Tpp1 intermediate with T39, K170, D206, and D218 indicates that their rate-limiting defect is in phosphoaspartate formation rather than hydrolysis.

The second asparate of PSP and dNT-2 motif I acts as an acid that donates a proton to the leaving group in the first phosphotransfer reaction and then as a base to extract a proton from a water molecule, making it a nucleophile for

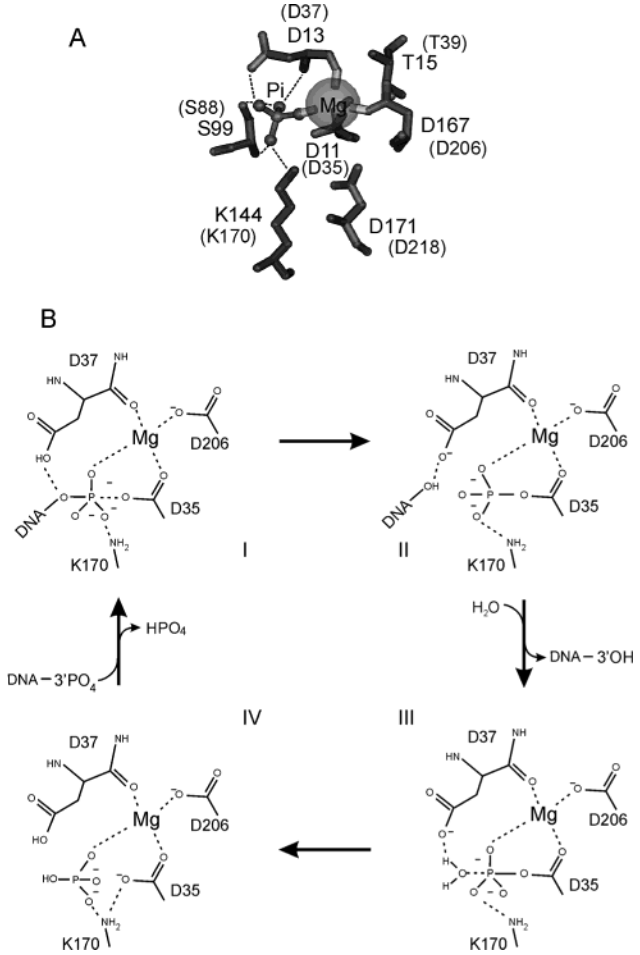

FIGURE 9: The proposed Tpp1 reaction mechanism. (A) Our results from activity and binding assays with Tpp1 mutants support an active site of Tpp1 that resembles Mj PSP. For reference, the drawing depicts the indicated residues from the crystal of Mj PSP in complex with P_i (generated using CN3D from the crystal; PDB number 1L7M) (*14*). The corresponding Tpp1 residues from Figure 1 are indicated in parentheses. (B) A model for Tpp1 catalysis can be proposed wherein D35 catalyzes removal of the 3′-phosphate, simultaneously forming a covalent intermediate. D37 acts as a proton donor for 3′-phosphate removal and as a proton acceptor activating a water molecule which attacks and cleaves the phospho-D35 intermediate. (I) DNA with the 3′-phosphate bound in the active site in a transition state with nucleophilic attack by D35. (II) Covalent phospho-Tpp1 intermediate through D35. (III) Transition state with a nucleophilic attack of a water molecule resulting in cleavage of the phospho-Tpp1 intermediate. (IV) Noncovalently bound phosphate after cleavage of the covalent intermediate.

phospoaspartate hydrolysis (*13*−*15*). Our results support a role for the equivalent residue of Tpp1, D37, in proton exchange. D37A showed very poor activity while D37E, capable of acid−base catalysis, retained substantial activity and covalent bond formation. Importantly, because this residue is involved in both phosphoaspartate formation and cleavage, it is not predictable whether mutants such as D37E would show an increased or decreased covalent intermediate. S88 is predicted to be positioned near D37 in the active site (*13*−*16*, *21*), and the analogous hPSP residue has been suggested to have a role in phosphoaspartate hydrolysis based on studies of its exchange reaction (*19*). Consistent with this, S88A showed a particularly strong detection of covalent intermediate.

The Basis of Tpp1 3′-Phosphate Specificity. Tpp1 is rigidly specific for removal of 3′-phosphates (*3*, *4*, *8*). It is entirely inactive at 3′-phosphoglycolate and 3′-aldehyde blocking lesions and is not an exo- or endonuclease. Contrary to our initial predictions, this does not appear to be a function of substrate binding. Tpp1 must be capable of accommodating more than just a 3′-phosphate in its active site, as shown by its binding to circular DNA. Instead, the inferred Tpp1 reaction mechanism (Figure 9B) provides an explanation for its substrate specificity. Specifically, the attack of D35 on the leaving phosphate is predicted to occur by an S_N2-type mechanism in which there is an inversion of the tetrahedral geometry around the phosphate via a trigonal-bipyramidal intermediate (*14*, *15*). A bulky and/or charged group on any one of the phosphate oxygens would thus need to be moved through the active site. The attendant steric and charge conflicts would be expected to impose severe restrictions on phosphate inversion, making cleavage impossible. Some degree of phosphoglycolate cleavage has been observed for bacterially purified plant homologues of Tpp1, although this was very weak (*33*, *34*). This would necessitate a significantly more open active site than seen in Tpp1, and indeed we have been unable to recapitulate this finding with highly active *Arabidopsis thaliana* zinc finger DNA 3′-phosphoesterase (AtZDP) protein purified from yeast (data not shown).

Mg^{2+} Binding and Charge Stabilization in the Tpp1 Active Site. The observation that Tpp1 binds stably to DNA allowed us to probe the defects of our active site mutants in considerable detail. Two observations indicate that this DNA binding occurs through the Tpp1 catalytic active site: binding of wild-type Tpp1 is Mg^{2+}-dependent, while D35 and D206 active site mutations largely abolish this Mg^{2+} dependence. These initially paradoxical observations emphasize that substrate binding, Mg^{2+} binding, and charge stabilization must be considered together. The active site of Tpp1 will have a high negative charge density because of the clustering of numerous aspartate residues and the substrate phosphate. This negative charge will be stabilized by the Mg^{2+} ion and also by positively charged active site amino acids, notably K170. Indeed, K170 mutants were neither active nor bound DNA. This includes the conservative K170R mutant, however, indicating that the function of K170 must extend beyond its charge to perhaps, based on comparison to PSP, positioning of the D35 side chain (*13*, *14*). We attribute the Mg^{2+} independence of DNA binding by D35A and D206A to the reduced charge density in the active site caused by these mutations. At the same time, the fact that DNA binding by D35A and D206A was only marginally enhanced in the presence of Mg^{2+} implies that these mutants are largely unable to bind Mg^{2+}. Thus, the effects of D35A and D206A mutations are twofold: they impair Mg^{2+} coordination but at the same time alleviate the need for the charge stabilization conferred by Mg^{2+}. These interpretations are supported by the fact that neither D35E nor D206E could bind DNA, even in the presence of Mg^{2+}, as they would disturb the Mg^{2+} coordination geometry while maintaining a negative charge.

Unlike D35 and D206, D37 is not implicated in Mg^{2+} binding. Its mutants showed a strong Mg^{2+} dependence for binding, and D37E in fact bound DNA most strongly. Importantly, we cannot exclude the contribution of other noncharged residues to Mg^{2+} binding, as they would not be expected to exhibit the loss of charge repulsion. However, PSP and related structures suggest that the remaining Mg^{2+}

coordination bonds are likely contributed by the backbone carbonyl of Tpp1 D37 and the phosphate itself (*13*−*15*).

Binding to the 3′ Terminus and Phosphate. Alanine mutants of two different residues showed an increase in DNA binding when a 3′-phosphate was present: D35A and D37A. Thus, Tpp1 must make binding contacts with the 3′-phosphate, and neither D35 nor D37 can be entirely responsible for these contacts. Mg^{2+} almost certainly contacts the phosphate via a coordinate bond, but this again is an insufficient explanation given the Mg^{2+} independence of D35A binding. Comparison with PSP structures suggests that S88 and K170 might contact the phosphate (*13*, *14*), but our binding data were not informative in this regard. D37 does appear to provide important contacts to the 3′ terminus, based on the particularly complex DNA binding pattern of its mutants. First, D37E was exceptional among mutants inferred to be Mg^{2+} binding competent in that it did show Mg^{2+}-independent binding, but only when a 3′-phosphate was present. This implies a strong functional interaction between the 37 position and the phosphate. However, an accounting must be made for the strong charge repulsion which would exist in such an active site. We argue that the longer glutamate side chain distorts the active site and pulls the phosphate from its normal position, especially in the absence of Mg^{2+} stabilization. Second, removal of the D37 side chain in D37A resulted in a nearly total loss of binding to the 3′-hydroxyl, but not 3′-phosphate, DNA. It thus appears that D37 becomes critical in the absence of the additional stabilizing contacts that can be made with the phosphate, again implicating D37 as a principal interactor with the 3′-hydroxyl.

Modes of DNA Binding by Tpp1. Although Tpp1 must bind DNA to carry out its function, we were surprised by the stability of this binding, especially on substrates without a 3′-phosphate or even a terminus. AtZDP was shown to bind DNA, but this had been attributed to a Zn-finger domain not present in Tpp1 (*34*). Tpp1 binding was largely specific to dsDNA, consistent with its described biological functions (*3*, *4*, *8*), but further substrate variations had lesser effects. Curiously, the 5′ terminated strand at a nick appeared inhibitory, despite the fact that Tpp1 is highly active at nicks (*8*). This likely reflects the fact that our EMSA assays fall short of what must presumably be the most active, but obligatorily transient, binding mode, a 3′-phosphate bound by wild-type enzyme with Mg^{2+} present. More specifically, our results suggest that Tpp1 engages DNA in a scanning mode, perhaps accompanied by translation along the DNA strand. Once a phosphate lesion is encountered, it is engaged in the active site. We hypothesize that the transition to the catalytic mode will require a conformational change that causes the active site to more completely encompass the DNA and simultaneously distorts its backbone, counteracting 5′ strand inhibition. A similar "open−closed" transition has been described for PSP (*14*). Proof of this hypothesis will require identification of Tpp1 residues outside of the active site that provide high-affinity DNA binding. These studies are in progress.

ACKNOWLEDGMENT

We thank Drs. Dindial Ramotar and Mats Ljungman for many helpful discussions and the members of the Wilson laboratory for their ongoing support and helpful comments on the manuscript.

REFERENCES

1. Friedberg, E. C., Walker, G. C., and Siede, W. (1995) *DNA Repair and Mutagenesis*, ASM Press, Washington, DC.
2. Johnson, A. W., and Demple, B. (1988) Yeast DNA 3′-repair diesterase is the major cellular apurinic/apyrimidinic endonuclease: substrate specificity and kinetics, *J. Biol. Chem. 263*, 18017−18022.
3. Vance, J. R., and Wilson, T. E. (2001) Repair of DNA strand breaks by the overlapping functions of lesion-specific and non-lesion-specific DNA 3′ phosphatases, *Mol. Cell. Biol. 21*, 7191−7198.
4. Karumbati, A. S., Deshpande, R. A., Jilani, A., Vance, J. R., Ramotar, D., and Wilson, T. E. (2003) The role of yeast DNA 3′-phosphatase Tpp1 and Rad1/Rad10 endonuclease in processing spontaneous and induced base lesions, *J. Biol. Chem. 278*, 31434−31443.
5. Midgley, C. A., and Murray, N. E. (1985) T4 polynucleotide kinase; cloning of the gene (pseT) and amplification of its product, *EMBO J. 4*, 2695−2703.
6. Karimi-Busheri, F., Daly, G., Robins, P., Canas, B., Pappin, D. J., Sgouros, J., Miller, G. G., Fakhrai, H., Davis, E. M., Le Beau, M. M., and Weinfeld, M. (1999) Molecular characterization of a human DNA kinase, *J. Biol. Chem. 274*, 24187−24194.
7. Jilani, A., Ramotar, D., Slack, C., Ong, C., Yang, X. M., Scherer, S. W., and Lasko, D. D. (1999) Molecular cloning of the human gene, PNKP, encoding a polynucleotide kinase 3′-phosphatase and evidence for its role in repair of DNA strand breaks caused by oxidative damage, *J. Biol. Chem. 274*, 24176−24186.
8. Vance, J. R., and Wilson, T. E. (2001) Uncoupling of 3′-phosphatase and 5′-kinase functions in budding yeast. characterization of *Saccharomyces cerevisiae* DNA 3′-phosphatase (Tpp1), *J. Biol. Chem. 276*, 15073−15081.
9. Koonin, E. V., and Tatusov, R. L. (1994) Computer analysis of bacterial haloacid dehalogenases defines a large superfamily of hydrolases with diverse specificity. Application of an iterative approach to database search, *J. Mol. Biol. 244*, 125−132.
10. Aravind, L., Galperin, M. Y., and Koonin, E. V. (1998) The catalytic domain of the P-type ATPase has the haloacid dehalogenase fold, *Trends Biochem. Sci. 23*, 127−129.
11. Collet, J. F., Stroobant, V., Pirard, M., Delpierre, G., and Van Schaftingen, E. (1998) A new class of phosphotransferases phosphorylated on an aspartate residue in an amino-terminal DXDX(T/V) motif, *J. Biol. Chem. 273*, 14107−14112.
12. Selengut, J. D. (2001) MDP-1 is a new and distinct member of the haloacid dehalogenase family of aspartate-dependent phosphohydrolases, *Biochemistry 40*, 12704−12711.
13. Wang, W., Kim, R., Jancarik, J., Yokota, H., and Kim, S.-H. (2001) Crystal structure of phosphoserine phosphatase from *Methanococcus jannaschii*, a hyperthermophile, at 1.8 A resolution, *Structure 9*, 65−71.
14. Wang, W., Cho, H. S., Kim, R., Jancarik, J., Yokota, H., Nguyen, H. H., Grigoriev, I. V., Wemmer, D. E., and Kim, S.-H. (2002) Structural characterization of the reaction pathway in phosphoserine phosphatase: crystallographic "snapshots" of intermediate states, *J. Mol. Biol. 319*, 421−431.
15. Rinaldo-Matthis, A., Rampazzo, C., Reichard, P., Bianchi, V., and Nordlund, P. (2002) Crystal structure of a human mitochondrial deoxyribonucleotidase, *Nat. Struct. Biol. 9*, 779−787.
16. Galburt, E. A., Pelletier, J., Wilson, G., and Stoddard, B. L. (2002) Structure of a tRNA repair enzyme and molecular biology workhorse: T4 polynucleotide kinase, *Structure 10*, 1249−1260.
17. Hisano, T., Hata, Y., Fujii, T., Liu, J.-Q., Kurihara, T., Esaki, N., and Soda, K. (1996) Crystal structure of L-2-haloacid dehalogenase from *Pseudomonas* sp. YL. An alpha/beta hydrolase structure that is different from the alpha/beta hydrolase fold, *J. Biol. Chem. 271*, 20322−20330.
18. Kim, Y., Yakunin, A. F., Kuznetsova, E., Xu, X., Pennycooke, M., Gu, J., Cheung, F., Proudfoot, M., Arrowsmith, C. H., Joachimiak, A., Edwards, A. M., and Christendat, D. (2004) Structure- and function-based characterization of a new phospho-

glycolate phosphatase from *Thermoplasma acidophilum*, *J. Biol. Chem. 279*, 517−526.
19. Collet, J. F., Stroobant, V., and Van Schaftingen, E. (1999) Mechanistic studies of phosphoserine phosphatase, an enzyme related to P-type ATPases, *J. Biol. Chem. 274*, 33985−33990.
20. Allegrini, S., Scaloni, A., Ferrara, L., Pesi, R., Pinna, P., Sgarrella, F., Camici, M., Eriksson, S., and Tozzi, M. G. (2001) Bovine cytosolic 5′-nucleotidase acts through the formation of an aspartate 52-phosphoenzyme intermediate, *J. Biol. Chem. 276*, 33526−33532.
21. Lahiri, S. D., Zhang, G., Dunaway-Mariano, D., and Allen, K. N. (2002) Caught in the act: the structure of phosphorylated beta-phosphoglucomutase from *Lactococcus lactis*, *Biochemistry 41*, 8351−8359.
22. Martzen, M. R., McCraith, S. M., Spinelli, S. L., Torres, F. M., Fields, S., Grayhack, E. J., and Phizicky, E. M. (1999) A biochemical genomics approach for identifying genes by the activity of their products, *Science 286*, 1153−1155.
23. Maxam, A. M., and Gilbert, W. (1980) Sequencing end-labeled DNA with base-specific chemical cleavages, *Methods Enzymol. 65*, 499−560.
24. Sugiyama, H., Fujiwara, T., Ura, A., Tashiro, T., Yamamoto, K., Kawanishi, S., and Saito, I. (1994) Chemistry of thermal degradation of abasic sites in DNA. Mechanistic investigation on thermal DNA strand cleavage of alkylated DNA, *Chem. Res. Toxicol. 7*, 673−683.
25. Bailly, V., Derydt, M., and Verly, W. G. (1989) δ-elimination in the repair of AP (apurinic/apyrimidinic) sites in DNA, *Biochem. J. 261*, 707−713.
26. Lhomme, J., Constant, J.-F., and Demeunynck, M. (1999) Abasic DNA structure, reactivity and recognition, *Biopolymers 52*, 65−83.
27. Wilson, T. E., Grawunder, U., and Lieber, M. R. (1997) Yeast DNA ligase IV mediates non-homologous DNA end joining, *Nature 388*, 495−498.
28. Pirard, M., Collet, J. F., Matthijs, G., and Van Schaftingen, E. (1997) Comparison of PMM1 with the phosphomannomutases expressed in rat liver and in human cells, *FEBS Lett. 411*, 251−254.
29. Collet, J. F., Gerin, I., Rider, M. H., Veiga-da-Cunha, M., and Schaftingen, E. V. (1997) Human L-3-phosphoserine phosphatase: sequence, expression and evidence for a phopshoenzyme intermediate, *FEBS Lett. 408*, 281−284.
30. Collet, J.-F., Stroobant, V., and Schaftingen, E. V. (2002) Evidence for phosphotransferases phosphorylated on aspartate residue in N-terminal DXDX(T/V) motif, *Methods Enzymol. 354*, 177−188.
31. Wang, L. K., and Shuman, S. (2002) Mutational analysis defines the 5′-kinase and 3′-phosphatase active sites of T4 polynucleotide kinase, *Nucleic Acids Res. 30*, 1073−1080.
32. Liu, J. Q., Kurihara, T., Miyagi, M., Tsunasawa, S., Nishihara, M., Esaki, N., and Soda, K. (1997) Paracatalytic inactivation of L-2-haloacid dehalogenase from *Pseudomonas* sp. YL by hydroxylamine. Evidence for the formation of an ester intermediate, *J. Biol. Chem. 272*, 3363−3368.
33. Betti, M., Petrucco, S., Bolchi, A., Dieci, G., and Ottonello, S. (2001) A plant 3′-phosphoesterase involved in the repair of DNA strand breaks generated by oxidative damage, *J. Biol. Chem. 276*, 18038−18045.
34. Petrucco, S., Volpi, G., Bolchi, A., Rivetti, C., and Ottonello, S. (2002) A nick-sensing DNA 3′-repair enzyme from *Arabidopsis*, *J. Biol. Chem. 277*, 23675−23683.

BI049434N